Supplementary

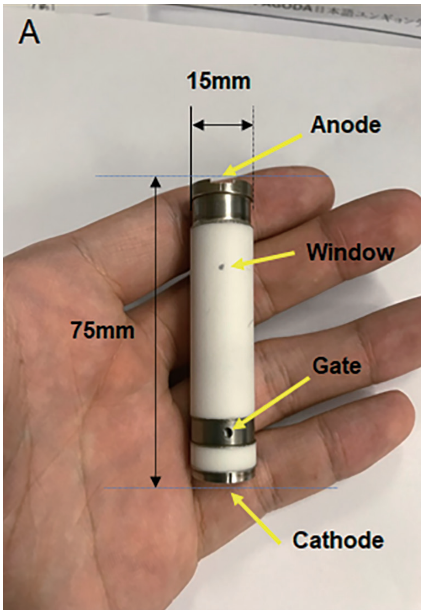

Figure S1 Carbon nanotube (CNT)-based X-ray source. The CNT X-ray source features a tri-polar structure comprising Anode, Cathode, and Gate. All the X-ray irradiations can be digitally controlled with high speed and high precision. Also, the CNT-based compact X-ray source can significantly reduce size and weight of the X-ray imaging device because the X-ray emission is performed via quantum tunneling of electrons without requiring any heating materials, such as filaments. Therefore, the CNT-based X-ray source is suitable option for developing intraoperative X-ray imager without causing any heat or power consumption issues during minimally invasive surgery.

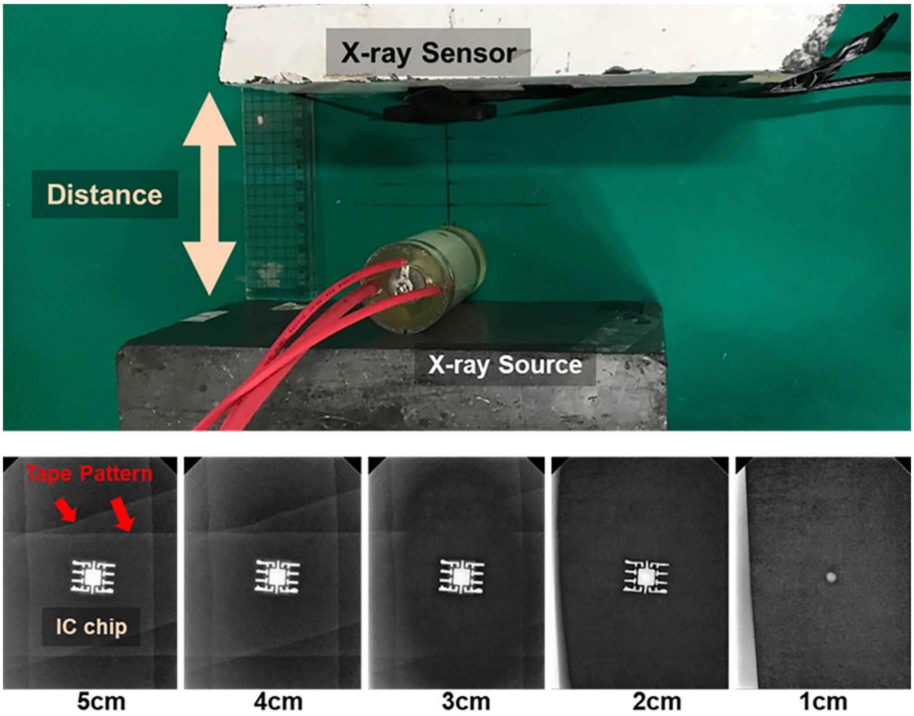

Figure S2 Experiment to determine the optimal distance between X-ray source and sensor. (A) Experimental setup; (B) X-ray images of an IC chip with different source-to-sensor distances (tube voltage =40 kVp, tube current =2 mA, exposure time =20 ms).

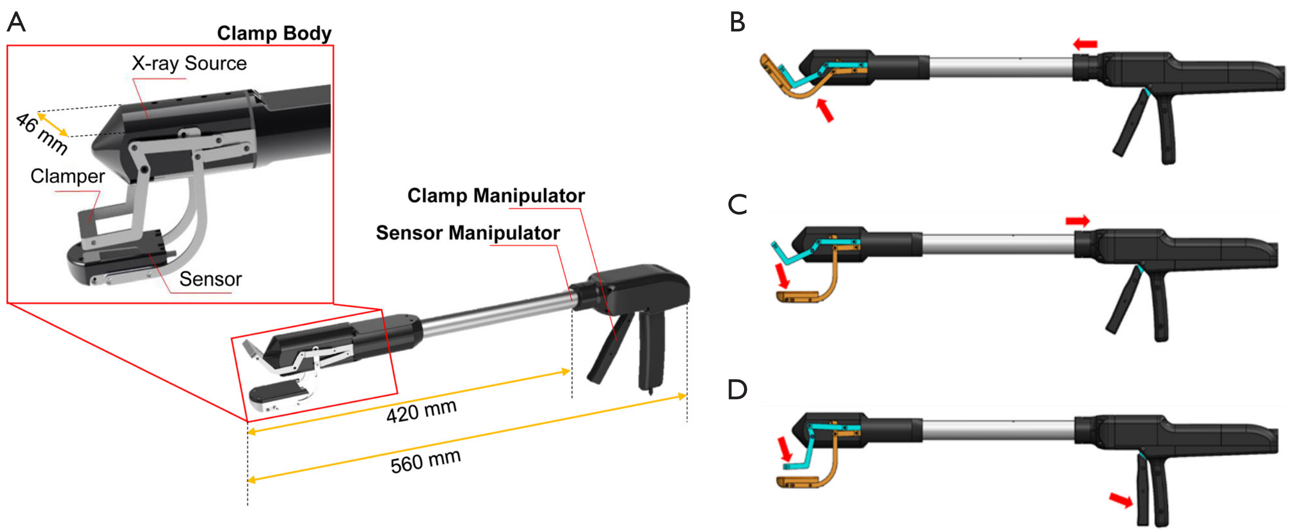

Figure S3 Drawing and operation protocol of the proposed intraoperative X-ray imager. (A) Drawing of the proposed device consisting of a clamp body, sensor manipulator, and clamp manipulator. Step-by-step operation protocol of the proposed device: (B) Insert mode, (C) Ready mode, and (D) Clamp mode.

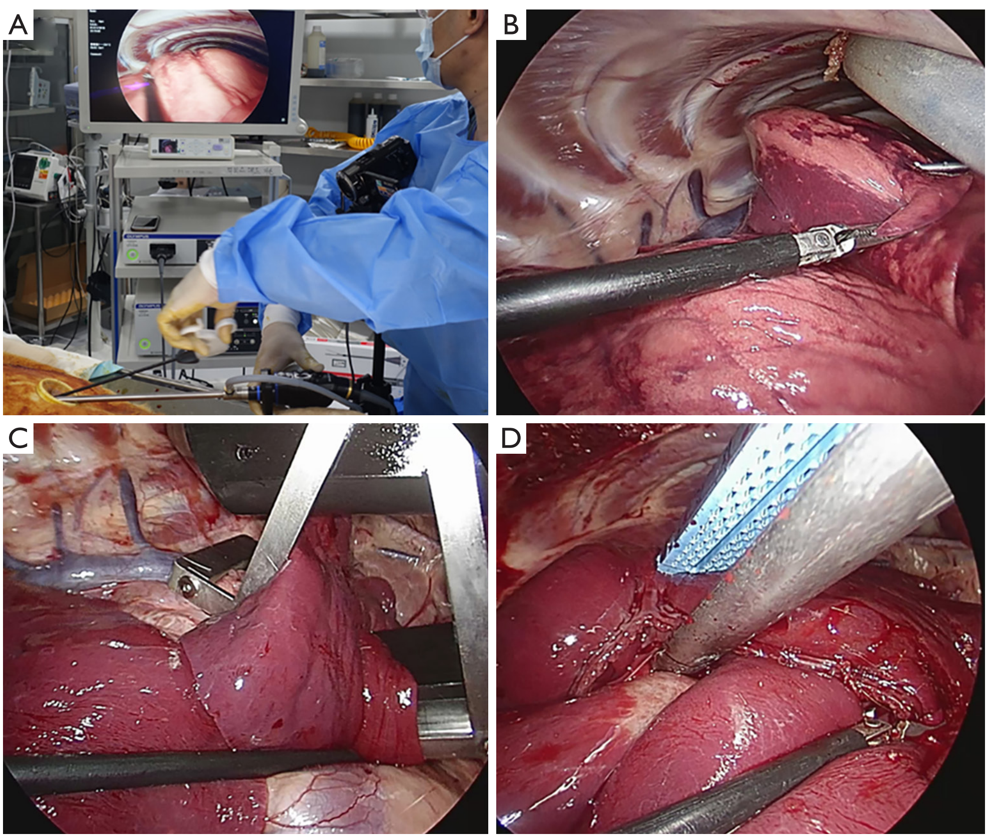

Figure S4 Minimally invasive thoracoscopic surgery in a dog to investigate the feasibility of the proposed X-ray imager. (A) Dog surgery; (B) localization with agar and Lipiodol; (C) detection of lung nodule with the X-ray device; (D) resection of the lesion by stapling.

 https://dx.doi.org/10.21037/tlcr-21-909

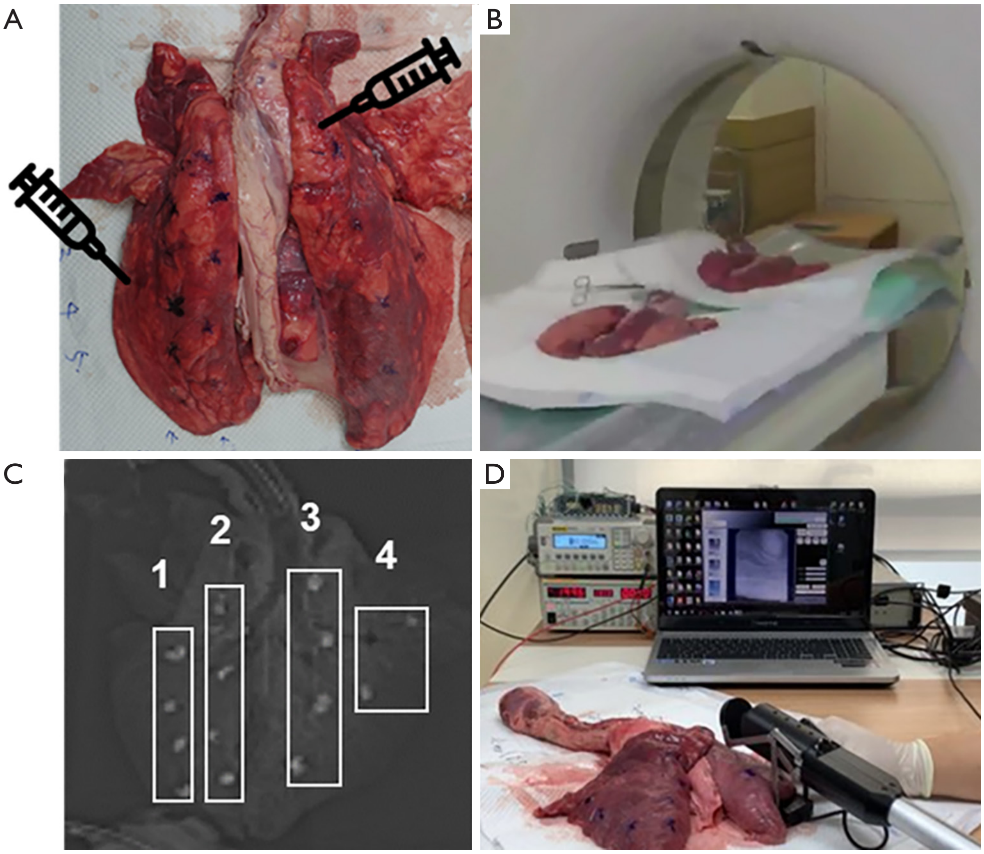

Figure S5 Lesion detectability assessment depending on the concentration of contrast agent and the depth of the lesion. (A) *Ex vivo* specimen of porcine lung tissue with pseudo lung nodules. (B) CT scanning. (C) Scout X-ray image of the lung acquired using the CT machine. The numbers above the boxes correspond to the groups summarized in *Table 1*. (D) Pseudo lung lesion scan using the proposed device.

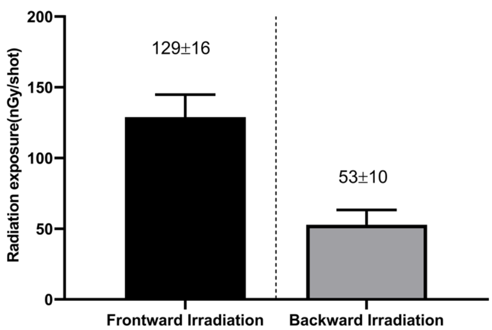

Figure S6 Equivalent radiation dose measured using a calibrated radiation dosimeter. The dosimeter was installed 1 m away from the X-ray focal spot, and the radiation dose was measured and averaged over 10 consecutive X-ray shots.

https://dx.doi.org/10.21037/tlcr-21-909

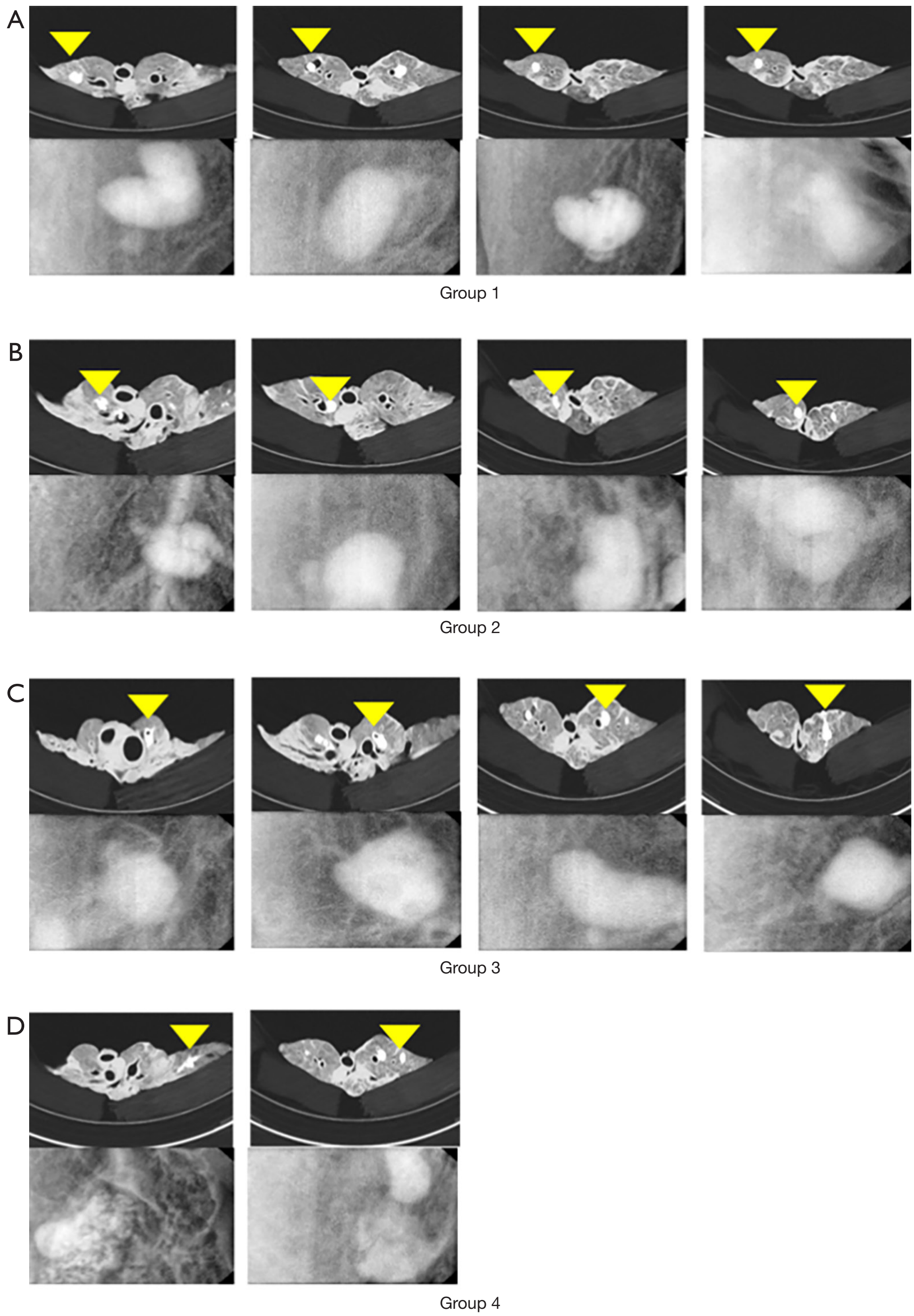

Figure S7 Comparison of X-ray images obtained using CT machine (up) and the proposed device (down). Pseudo lung lesions in pigs were created with different volumes of an agar/Lipiodol mixture and in different pleural depths. (A) Group 1: 1 mL and 0.5 cm. (B) Group 2: 2 mL and 0.5 cm. (C) Group 3: 1 mL and 1 cm. (D) Group 4: 2 mL and 1 cm.

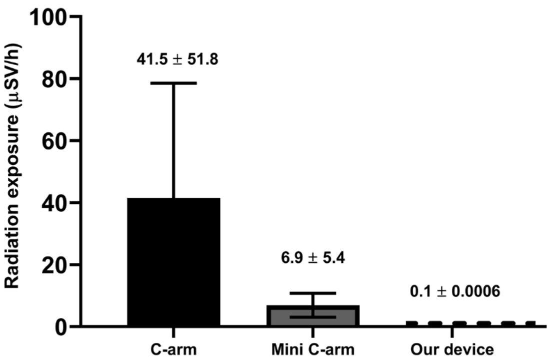

Figure S8 Radiation exposure during intraoperative real-time X-ray imaging for pseudo lung lesion detection with radiocontrast agent. Our device (0.1±0.0006 μSv/h) yielded the lowest radiation exposure as compared to the conventional C-arm fluoroscopy (41.5±51.8 μSv/h) and mini C-arm used for dental or hand surgery (6.9±5.4 μSv/h).

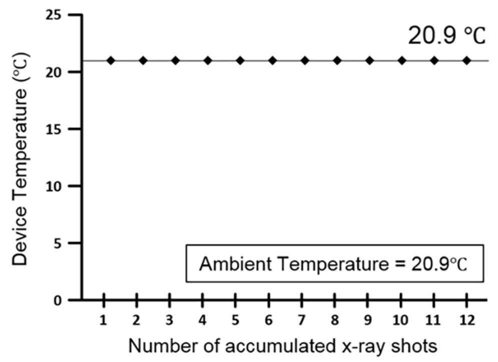

Figure S9 Temperature measurements of the proposed device while performing 12 consecutive X-ray irradiations every 5 s. The parameters for X-ray irradiation were identical to those for other imaging experiments with a tube voltage of 40 kVp, a tube current of 2 mA, and an exposure time of 20 ms.

Table S1 SNR values of detected pseudo lung lesions in the X-ray image

	Group 1	Group 2	Group 3	Group 4
1st row	14.39	16.22	18.28	19.28
2nd row	17.70	17.96	15.27	17.32
3rd row	17.34	19.95	14.52	N/A
4th row	14.51	17.04	14.90	N/A

SNR, signal-to-noise ratio (unit: dB); N/A, not applicable.

https://dx.doi.org/10.21037/tlcr-21-909